Neurobiology of Disease 179 (2023) 106055

Contents lists available at ScienceDirect

Neurobiology of Disease

journal homepage: www.elsevier.com/locate/ynbdi

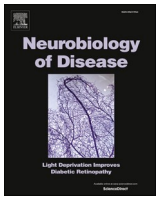

Dynamic flexibility and controllability of network communities in juvenile myoclonic epilepsy

Anatolie Vataman [a,b,c], Dumitru Ciolac [a,b,c], Vitalie Chiosa [b,c], Daniela Aftene [b,c], Pavel Leahu [b,c], Yaroslav Winter [d], Stanislav A. Groppa [b,c], Gabriel Gonzalez-Escamilla [a], Muthuraman Muthuraman [a,1], Sergiu Groppa [a,*,1]

[a] Department of Neurology, Focus Program Translational Neuroscience (FTN), Rhine-Main Neuroscience Network (rmn^2), University Medical Center of the Johannes Gutenberg University Mainz, Mainz, Germany
[b] Laboratory of Neurobiology and Medical Genetics, Nicolae Testemițanu State University of Medicine and Pharmacy, Chisinau, Republic of Moldova
[c] Department of Neurology, Institute of Emergency Medicine, Chisinau, Moldavia
[d] Mainz Comprehensive Epilepsy and Sleep Medicine Center, Department of Neurology, Johannes Gutenberg University Mainz, Mainz, Germany

ARTICLE INFO

Keywords:
Juvenile myoclonic epilepsy
Network community
Flexibility
Controllability

ABSTRACT

Juvenile myoclonic epilepsy (JME) is the most common syndrome within the idiopathic generalized epilepsy spectrum, manifested by myoclonic and generalized tonic-clonic seizures and spike-and-wave discharges (SWDs) on electroencephalography (EEG). Currently, the pathophysiological concepts addressing SWD generation in JME are still incomplete. In this work, we characterize the temporal and spatial organization of functional networks and their dynamic properties as derived from high-density EEG (hdEEG) recordings and MRI in 40 JME patients (25.4 ± 7.6 years, 25 females). The adopted approach allows for the construction of a precise dynamic model of ictal transformation in JME at the cortical and deep brain nuclei source levels. We implement Louvain algorithm to attribute brain regions with similar topological properties to modules during separate time windows before and during SWD generation. Afterwards, we quantify how modular assignments evolve and steer through different states towards the ictal state by measuring characteristics of flexibility and controllability. We find antagonistic dynamics of flexibility and controllability within network modules as they evolve towards and undergo ictal transformation. Prior to SWD generation, we observe concomitantly increasing flexibility ($F(1,39) = 25.3$, corrected $p < 0.001$) and decreasing controllability ($F(1,39) = 55.3$, $p < 0.001$) within the fronto-parietal module in γ-band. On a step further, during interictal SWDs as compared to preceding time windows, we notice decreasing flexibility ($F(1,39) = 11.9$, $p < 0.001$) and increasing controllability ($F(1,39) = 10.1$, $p < 0.001$) within the fronto-temporal module in γ-band. During ictal SWDs as compared to prior time windows, we demonstrate significantly decreasing flexibility ($F(1,14) = 31.6$; $p < 0.001$) and increasing controllability ($F(1,14) = 44.7$, $p < 0.001$) within the basal ganglia module. Furthermore, we show that flexibility and controllability within the fronto-temporal module of the interictal SWDs relate to seizure frequency and cognitive performance in JME patients. Our results demonstrate that detection of network modules and quantification of their dynamic properties is relevant to track the generation of SWDs. The observed flexibility and controllability dynamics reflect the reorganization of de−/synchronized connections and the ability of evolving network modules to reach a seizure-free state, respectively. These findings may advance the elaboration of network-based biomarkers and more targeted therapeutic neuromodulatory approaches in JME.

Abbreviations: BDI-II, Beck Depression Inventory (2nd edition); FA, flip angle; FEM, finite-element method; FoV, field of view; FLAIR, fluid attenuated inversion recovery; HAM-A, Hamilton Anxiety scale; hdEEG, high-density electroencephalography; JME, juvenile myoclonic epilepsy; LFM, lead-field matrix; MoCA, Montreal Cognitive Assessment scale; ROI, region of interest; ST, slice thickness; SWD, spike-and-wave discharge; TE, echo time; TI, inversion time; TR, repetition time.

* Corresponding author at: Department of Neurology, Focus Program Translational Neuroscience (FTN), Rhine-Main Neuroscience Network (rmn^2), University Medical Center of the Johannes Gutenberg University Mainz, Langenbeckstrasse 1, 55131 Mainz, Germany.
E-mail address: segroppa@uni-mainz.de (S. Groppa).
[1] These authors contributed equally to this work.

https://doi.org/10.1016/j.nbd.2023.106055
Received 27 October 2022; Received in revised form 3 February 2023; Accepted 22 February 2023
Available online 25 February 2023

1. Introduction

Juvenile myoclonic epilepsy (JME), the most common syndrome within the idiopathic generalized epilepsy (IGE) spectrum, is characterized by occurrence primarily of myoclonic seizures and bilateral synchronous spike/polyspike-wave complexes (i.e. spike-and-wave discharges or SWDs) on electroencephalography (EEG) (Beniczky et al., 2012). Spike-and-wave discharges in JME have been postulated to arise from an abnormal oscillatory activity of neuronal populations within the cortico-subcortical networks (Assenza et al., 2020; Groppa et al., 2008). Particularly, dysfunction of thalamo-frontal circuits was proposed as a key mechanism in the generation of SWDs (O'Muircheartaigh et al., 2012; Jiang et al., 2018; Groppa et al., 2012); however, other cortical regions from parietal, temporal, and occipital lobes were also shown to be involved (Caeyenberghs et al., 2015; Lee et al., 2017; Moeller et al., 2013). At the same time, widespread cortical alterations have been observed in the time period preceding the SWD generation, mainly involving the regions belonging to the default-mode network and the sensory-motor network (Clemens et al., 2013; Benuzzi et al., 2012). In our recent work focusing on interictal discharges in patients with focal epilepsy, we demonstrated alpha and theta band-driven connectivity alterations before spike generation within the fronto-temporo-thalamic networks (Chiosa et al., 2017). Thus, network alterations occurring prior to the generation of epileptic discharges may offer valuable clues into the subsequent transition to a seizure state.

Seizure state transition is characterized by a dynamic network reconfiguration across the involved brain regions known as network communities. Two network characteristics have been proposed to describe this network reconfiguration – flexibility (Khambhati et al., 2015) and controllability (Scheid et al., 2021). Flexibility, i.e. frequency with which a functionally-defined region of interest changes its assigned community over time, was shown to decrease as the networks evolve from a pre-seizure to a seizure state in patients with neocortical epilepsy (Khambhati et al., 2015). Controllability, i.e. the ability of a network to be driven through a range of different states towards a specific state, was shown to increase beginning with the preictal and throughout the ictal states in patients with focal epilepsy (Scheid et al., 2021). So far, network communities and their dynamic properties, flexibility and controllability, during network state transitions have not been addressed in patients with JME and their elucidation may advance the elaboration of target, brain state-dependent neuromodulatory approaches.

Aiming to identify network alterations occurring during seizure state transitions in JME patients, we test the following hypotheses: i) specific network communities are involved in generation and propagation of interictal and ictal SWDs across the cortico-subcortical networks, and ii) dynamic properties (i.e. flexibility and controllability) of network communities alter as they transit to interictal or ictal state. We test these hypotheses in JME patients by estimating the oscillatory brain activity on source level and quantifying dynamic alterations of network communities before and during the occurrence of interictal/ictal SWDs, based on high-density EEG (hdEEG, 256 electrodes) recordings and magnetic resonance images (MRI).

2. Materials and methods

2.1. Study participants

In a cohort of 3280 patients with epilepsy evaluated in the outpatient epilepsy department of the Tertiary University Center, Chisinau, Republic of Moldova, 207 patients with myoclonic seizures were identified, among which 40 patients met the criteria of JME and were included into the study. Definition of JME was based on the current International League Against Epilepsy classification (Scheffer et al., 2017) and consensus on diagnosis and management of JME (Trenité et al., 2013). Exclusion criteria were significant comorbidity, metabolic disorders, alcohol and substance abuse, and any other medical conditions known to significantly modify the background EEG activity. All patients had previously undergone standard EEG examination as part of their routine diagnostic work-up. For this study, hdEEG and high-resolution MRI were performed in all patients. Demographical and clinical data of patients are summarized in Table 1. The study protocol was approved by the local ethical committee and all participants gave written informed consent prior to the study inclusion.

2.1.1. Neuropsychological assessment

Neuropsychological assessment included the Montreal Cognitive Assessment (MoCA) scale, the Hamilton Anxiety (HAM-A) scale, and the Beck Depression Inventory (2nd edition, BDI-II). The MoCA (total score range 0–30) is a rapid screening tool aimed to evaluate different cognitive domains, including attention and concentration, executive functions, memory, language, visuoconstructional skills, conceptual thinking, calculations, and orientation (Nasreddine et al., 2005) HAM-A (total score range 0–56) consists of 14 items that measure the severity of anxiety (Hamilton, 1959). The BDI-II test (total score range 0–63) consists of 21 items that assess presence and intensity of depression symptoms (Beck et al., 1996).

2.2. MRI acquisition

All participants were imaged at a 3 T MRI scanner (Siemens Magnetom Skyra) using a 32-channel head coil according to a predefined Epilepsy protocol (Chiosa et al., 2017; Chiosa et al., 2019), with the following imaging sequences: T1-weighted image (repetition time [TR] = 2000 ms, echo time [TE] = 9 ms, inversion time [TI] = 900 ms, slice thickness [ST] = 4 mm, flip angle [FA] = 9°, field of view [FoV] = 256 × 256 mm^2, acquisition matrix = 256 × 256), T2-weighted images (TR = 3800 ms, TE = 117 ms, ST = 4 mm, FA = 149°, FoV = 100 × 100 mm^2, acquisition matrix = 384 × 384), and 3D fluid-attenuated inversion recovery (FLAIR) images (TR = 5.000 ms, TE = 388 ms, TI = 1.800 ms, ST = 0.9 mm, FA = 120°, FoV = 100 × 100 mm^2, acquisition matrix = 256 × 256). Particular attention was taken to center the subject in the head coil and to restrain head movements with cushions and adhesive medical tape. All patients reported no seizure during the scanning procedure.

2.3. High-density EEG acquisition

High-density EEG recordings were performed in the morning (08:00–10:00 AM) at rest and in an alert state for two hours in a dimly lit

Table 1
Demographical and clinical parameters of patients.

	JME patients (n = 40)
Gender (female / male)	25 (62%) / 15 (38%)
Age (years)	25.4 ± 7.6 years
Handedness (right / left)	37 (92%) / 3 (8%)
Age at epilepsy onset (years)	14.2 ± 7.1 years
Disease duration (years)	10.4 ± 7.4 years
Seizure semiology	MS – 40 (100%), GTCS – 34 (85%), AS – 11 (28%)
Frequency of myoclonic seizures (seizures/month)	2 [1–40]
MoCA	25.1 ± 4.7
HAM-A	9.9 ± 6.8
BDI-II	8.7 ± 6.7
Antiseizure medication	VPA – 31 (78%), LTG – 19 (48%), CZP – 2 (5%), CLB – 1 (3%)

Data are presented as mean ± standard deviation, median [range] or absolute numbers (%).
AS – absence seizure; BDI-II – Beck Depression Inventory (2nd edition); CLB – clobazam; CZP – clonazepam; GTCS – generalized tonic-clonic seizure; HAM-A – Hamilton Anxiety scale; LEV – levetiracetam; LTG – lamotrigine; MoCA – Montreal Cognitive Assessment scale; MS – myoclonic seizure; VPA – valproate.

and quiet room. The EEG electrodes were placed according to the international 10/5 system and included in a special net with 20–25 mm interelectrode distance (HydroCel Geodesic Sensor Net 130, 256 electrodes, MagstimEGI) and in reference to anatomical landmarks. The sampling rate of recordings was set to 1000 Hz and the electrodes' impedance was kept below 50 kΩ. The acquired raw data recordings were filtered offline by using the tools integrated into the Net Station 5 software package. The notch filter was set at 50 Hz to avoid line interference, and the low cutoff filter was set at 1 Hz (using a 4th order Butterworth filter) to remove slow drifts into the data. The high cutoff filter was set at 70 Hz (through a 4th order Butterworth filter) to remove the channels contaminated with high-frequency activities. Subsequently, the filtered data were used to visually identify and manually select the SWDs.

Spike-and-wave discharges occurring without observable clinical seizures were considered as interictal discharges and SWDs followed by myoclonic jerks were considered as ictal discharges. Individual hdEEG recordings were visually checked by trained neurophysiologists (AV and VC) and a total of 643 primary generalized interictal SWDs in all patients and 80 ictal SWDs in 15 patients were identified. To avoid data contamination, SWDs only with artifact-free epochs 15 s before and 15 s after the discharges were manually selected. Following this step, the onset and offset of 340 interictal and 73 ictal SWDs were marked and included into subsequent analysis (individual numbers of SWDs as well as their duration in each patient are provided in Supplementary Table 1).

2.4. EEG preprocessing

Preprocessing of the hdEEG data and part of the spatial filter analysis were carried out in MATLAB2015a and FieldTrip toolbox (Oostenveld et al., 2011). The adopted preprocessing pipeline from the FieldTrip toolbox is explained elsewhere (Liu et al., 2011). As a first step, hdEEG data containing interictal SWDs were analyzed. For this, hdEEG data were re-referenced to the common grand average reference of all EEG channels and epoched into 20 s for each patient separately - 15 s before the interictal SWD (pre-SWD time window) and 5 s including the SWD (SWD time window) (Fig. 1). Subsequently, the pre-SWD time window was subdivided into three time windows: the time interval from 15 to 10 s was defined as the pre-SWD-15 time window, the time interval from 10 to 5 s as the pre-SWD-10 time window, and the time interval of 5 s just before the SWD was defined as the pre-SWD-5 time window. Eventually, before and during interictal SWDs, four time windows were analyzed: pre-SWD-15, pre-SWD-10, pre-SWD-5, and interictal SWD time windows. As a second step, a similar approach was adopted to the epochs with ictal discharges, resulting in following time windows: pre-SWD-15, pre-SWD-10, pre-SWD-5, and ictal SWD time windows. The entire 20 s epochs were fed into independent component analysis (FastICA) to remove the components representing the exponential decay artifact, residual muscle artifacts, eye blinks, eye movements, line noise, and

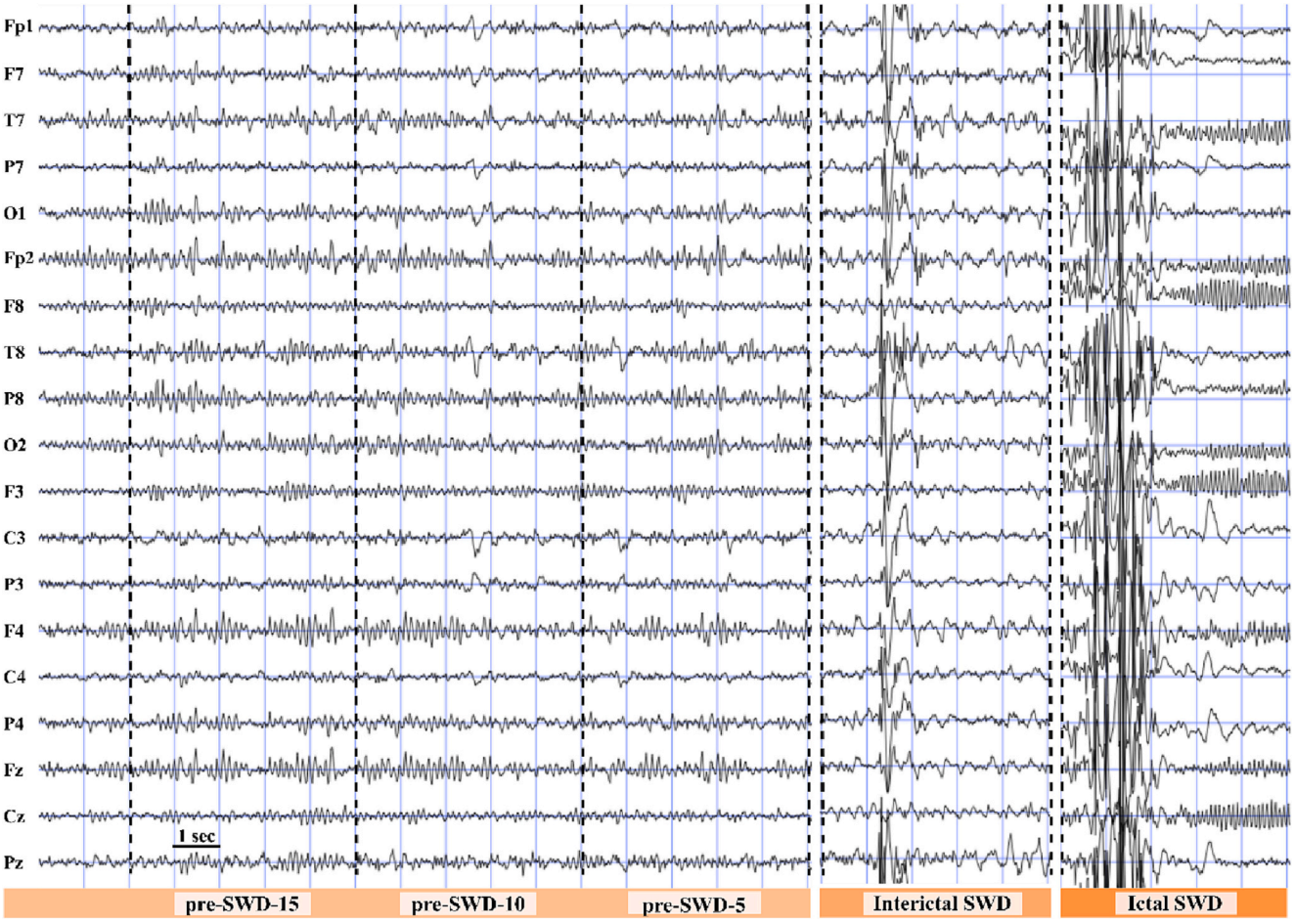

Fig. 1. The analyzed time windows. High-density EEG recordings were epoched into non-overlapping 5 s long time windows: three windows before the interictal or ictal SWDs (pre-SWD-15, pre-SWD-10, and pre-SWD-5 time windows) and one window during the SWDs (interictal or ictal SWD time window). Interictal SWDs denote discharges without ongoing seizures and ictal SWDs denote discharges during the myoclonic seizures. Spaces before the interictal and ictal SWD time windows indicate that the three pre-SWD time windows were analyzed separately before interictal and separately before ictal SWDs. For simplicity, electrodes in the figure are represented in the international 10–20 system montage.

other muscle artifacts. Selection of 20 s long epochs (15 s before and 5 s during SWDs) with subsequent subdivision into 5 s long time windows was based on empirical data indicating significant network dynamics peaking at 5 seconds (Chiosa et al., 2017; Tangwiriyasakul et al., 2018; Gupta et al., 2011) and accompanying vascular changes (Benuzzi et al., 2012; Moeller et al., 2008) over the 10 s interval before the generation of interictal and ictal discharges.

2.4.1. Reconstruction of brain activity

To reconstruct the brain activity on source level, an established procedure was applied by estimating the lead-field matrix (LFM) with specified models for the brain, the finite-element method (FEM) (Wolters et al., 2007). For forward modeling, surfaces of the compartments such as skin, skull, cerebrospinal fluid, and gray and white matter were extracted from individual T1-weighted MRI scans. The forward modeling and source analysis were performed in FieldTrip (Oostenveld et al., 2011). The LFM contains the information about the geometry and conductivity of the FEM model. The output of the beamformer at a voxel in the brain can be defined as a weighted sum of the output of all EEG channels. The weights determine the spatial filtering characteristics of the beamformer and are selected to increase the sensitivity to signals from a voxel and reduce the contributions of signals from (noise) sources at different locations. In order to visualize power at a given frequency range, a linear transformation was used based on a constrained optimization problem, which acts as a spatial filter (Van Veen et al., 1997). The spatial filter assigned a specific value of power to each voxel. For a given source, the beamformer weights for a location of interest are determined by the data covariance matrix and the LFM. In this study, to extract the sources of the whole-brain activity, we adopted a data-driven approach that was previously implemented successfully (Gonzalez-Escamilla et al., 2023; Sabbagh et al., 2020; Dähne et al., 2014). A voxel size of 5 mm was used, resulting in 6676 voxels covering the entire brain. The created source model was spatially normalized to the MNI space and mapped to 111 brain regions of interest (ROIs), defined according to the Harvard-Oxford atlas (96 cortical and 15 subcortical regions) according to (Gollo et al., 2017). Once regional voxels were identified, their activity was extracted from the source space. Initially, a grand average power spectrum was estimated over the all regions from all subjects within EEG epochs with SWDs and epochs without SWDs. Following this analysis, significant differences in power between the epochs were attested only in beta (13–30 Hz) and gamma (31–50 Hz) frequency bands. We opted for an upper limit of 50 Hz within the gamma band, since epileptic discharges recorded from surface EEG mainly occur in the frequency range from 0.5 to 50 Hz (Zhang et al., 2019; Swami et al., 2019). Subsequently, for each frequency band, the activated voxels were selected by a within-subject surrogate analysis to define the significance level. The surrogate analysis was based on a 5 s windowing, which can identify the significant regions of activation for each individual patient. The number of surrogates was adequate with bootstrapping of a 1 s window within the 5 s period (Mader et al., 2013).

2.5. Network analysis (community detection)

Based on the reconstructed brain activity, individual weighted connectivity matrices were obtained for beta and gamma power separately. Within the connectivity matrices, each link represented the correlation coefficient between beta or gamma power in a particular ROI (*j*) to each of the other ROIs (*i*). Previously, we have effectively implemented this approach on EEG data (Gonzalez-Escamilla et al., 2023). Other studies as well have successfully applied the source power co-modulation on EEG data for delineating the network information (Sabbagh et al., 2020; Dähne et al., 2014). After constructing the connectivity matrices, network dynamics were characterized by using a set of measures (see below) as implemented in the brain connectivity toolbox (Rubinov and Sporns, 2010) and the dynamics graph metrics toolbox (Sizemore and Bassett, 2018).

Network communities (modules) were identified by applying the Louvain modularity algorithm (Blondel et al., 2008) in each individual subject's connectivity matrix. To test the robustness of the detected community association at each time interval, we performed 5000 iterations with the Louvain algorithm, where the assignment of each region to a particular community was based on the maximum number of times/iterations a region was assigned to a community (Ritchey et al., 2014). During this process γ, which is the resolution parameter, varied from 1 to 2.5 in steps of 0.05 to identify a stable γ value that can be used for further time windows. Given the individual variability of the identified modules in each time window, a group community structure for each time window was obtained across all subjects.

2.5.1. Network measures

For each network community, two network measures were assessed – controllability and flexibility.

Flexibility is defined as frequency with which a functionally-defined region of interest (node) changes its assigned community over time and normalized by the total number of changes that were possible (Bassett et al., 2011). For each network community, mean flexibility over all nodes of the respective community was calculated.

Controllability of a network denotes the ability of a node to influence other nodes and is calculated as the average input energy from a set of control nodes required to reach all the possible states of the system (i.e., the entire magnitude of energy measured across all nodes) (Scheid et al., 2021; Gu et al., 2015). For each network node, the input energy was calculated by computing the trace of the inverse of the controllability Gramian – $Trace(W_k^{-1})$: $W_k = \sum_{\tau=0}^{\infty} A^{\tau} B_k B_k^T A^{T\tau}$, where input matrix B_k identifies the control points *k* in the brain, and *A* is the adjacency matrix (Scheid et al., 2021).

To assess the topological architecture between the network communities, we calculated the average *clustering coefficient*. The average clustering coefficient is a global measure of network segregation and reflects the clustered connections around individual nodes (Rubinov and Sporns, 2010). Here, the clustering coefficient was calculated by the algorithm as implemented in Onnela (Onnela et al., 2005). In case a node had only one edge or no edges, the clustering coefficient was set to zero.

2.6. Statistical analysis

Normal distribution of the data (demographic, clinical, network) was checked using the Shapiro-Wilk tests. Analysis on the dynamic changes of the network measures across the selected time windows was performed separately for interictal and ictal SWDs. Before entering into the general linear model, network measures (flexibility, controllability, and clustering coefficient) were averaged across all of the selected individual time windows (separately for pre-SWD-15, pre-SWD-10, pre-SWD-5, and interictal/ictal SWD time windows) in each patient, thus resulting in one value of the network measure per patient, per time window, and per module. Afterwards, network measures (as dependent variables) were compared across the four time windows (as independent variable with four levels: pre-SWD-15, pre-SWD-10, pre-SWD-5, and interictal or ictal SWD time windows) by means of repeated measures analysis of covariance (ANCOVA) controlling for age, sex, disease duration, number of antiseizure medications, and number of interictal or ictal SWDs. At this stage, the ANCOVA models were followed by a Greenhouse–Geisser correction for lack of sphericity and post hoc tests with a Bonferroni correction to adjust for multiple comparisons. The association between clinical variables (disease duration, frequency of myoclonic seizures, MoCA, HAM-A, and BDI-II) and network measures (controllability, flexibility) was assessed by applying linear regression models controlling for age and gender. Additionally, support vector regressions were used to assess the accuracy of network parameters to predict clinical variables. *P*-values below 0.05 were considered statistically significant. Statistical analysis was conducted in MATLAB2015a (Mathworks,

Natick, Mass) and SPSS software (version 21.0; IBM, Armonk, NY, USA.).

3. Results

3.1. Subject characteristics

The mean age of included subjects was 25.4 ± 7.6 years with a mean disease duration of 10.4 ± 7.4 years (Table 1). All subjects presented myoclonic seizures (100%) and majority of them generalized tonic-clonic seizure (85%), while a few had absence seizures (28%) as well. Valproate was the most commonly (31/40) administered antiseizure medication. Twenty-eight (70%) patients were on monotherapy and 12 (30%) were receiving polytherapy (≥ 2 antiseizure medications). The MRI examination was unremarkable in all patients. The median number of recorded interictal discharges was 11 (1–65) with an average duration of 0.314 ± 0.377 s. The median number of ictal discharges was 1 (0–45) with an average duration of 1.240 ± 0.654 s (Supplementary Table 1).

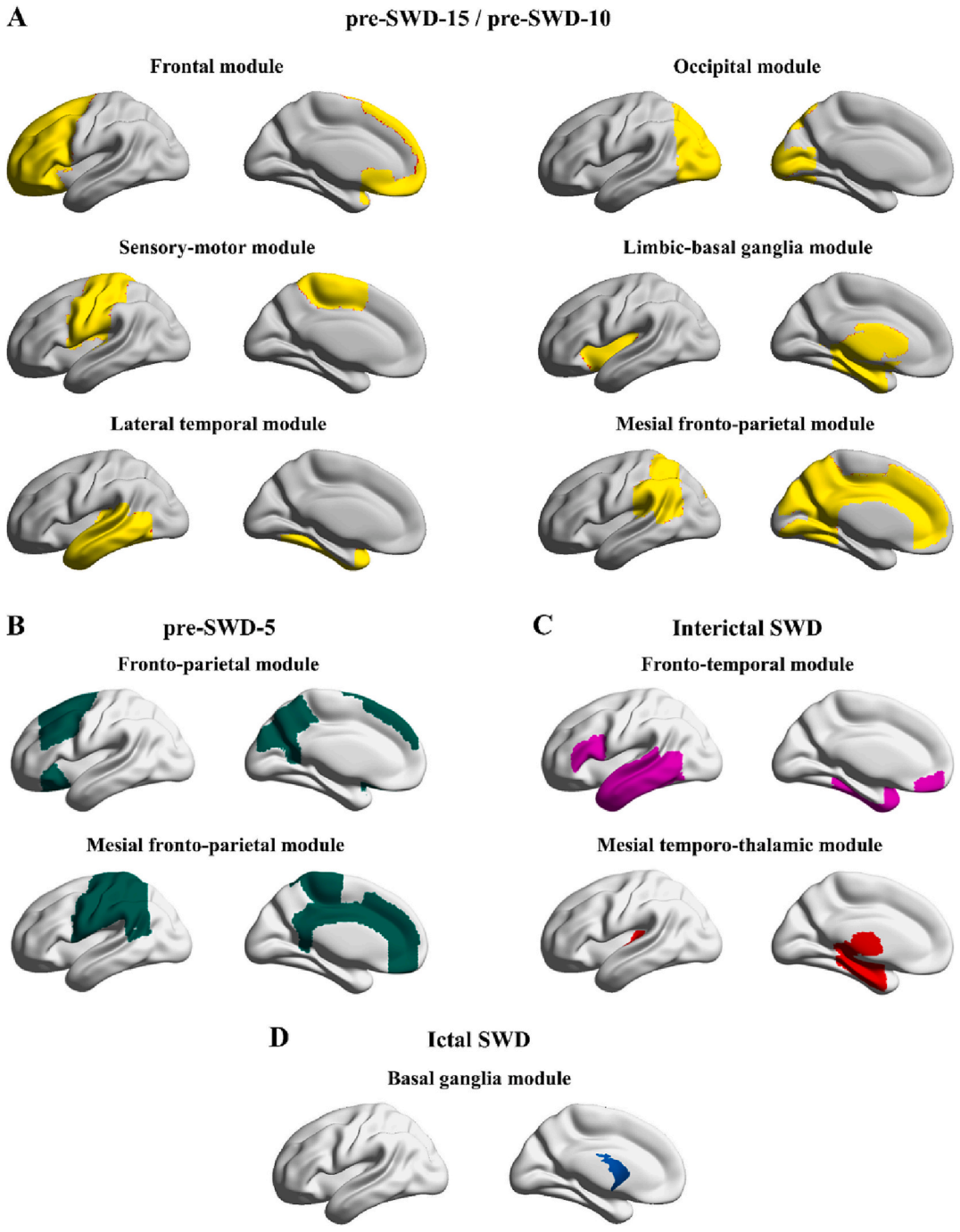

Fig. 2. Group representation of network communities in each time window. In the pre-SWD-15 and pre-SWD-10 time windows, six modules were identified in gamma and beta frequency bands (A). In the pre-SWD-5 time window, one additional module in gamma and two additional modules in beta frequency band were identified (B). In the interictal SWD time window, one additional module in gamma and two additional modules in beta frequency band were identified (C). In the ictal SWD time window, only one additional module, the basal ganglia module (without thalamus), was identified in both frequency bands (D).

3.2. Network community assignments of generalized discharges

3.2.1. Network communities before and during interictal discharges

In gamma and beta frequency bands, six modules were identified in the pre-SWD-15 time window - frontal module (comprising mainly lateral frontal lobe areas), sensory-motor module (comprising mainly precentral and postcentral cortices), lateral temporal module (comprising mainly lateral temporal lobe areas), occipital module (comprising mainly lateral occipital lobe and visual areas), limbic-basal ganglia module (comprising mainly insula and basal ganglia), and mesial fronto-parietal module (comprising mainly mesial frontal and lateral and medial parietal lobe areas) (Fig. 2A). The same six modules were as well observed in the pre-SWD-10 time window in both gamma and beta frequency bands (Fig. 2A).

In gamma frequency band, in the pre-SWD-5 time window, one additional module (to those six modules identified in the preceding two time windows) was found – fronto-parietal module (comprising mainly lateral frontal and medial parietal lobe areas) (Fig. 2B). In the interictal SWD time window, one additional module (to those seven identified in the preceding three time windows) was attested – fronto-temporal module (comprising mainly inferior frontal and lateral temporal lobe areas) (Fig. 2C). Eventually, in gamma frequency band in the interictal SWD time window, eight modules were detected.

In beta frequency band, in the pre-SWD-5 time window, two additional modules (to those six modules identified in the preceding pre-SWD-15 and pre-SWD-10 time windows) were found – fronto-parietal module and mesial fronto-parietal module (comprising mainly mesial frontal, sensory-motor, and lateral parietal lobe areas) (Fig. 2B). In the interictal SWD time window, two additional modules (to those eight identified in the preceding pre-SWD-15, pre-SWD-10 and pre-SWD-5 time windows) were attested – fronto-temporal module and mesial temporo-thalamic module (comprising mainly hippocampus, amygdala, and thalamus) (Fig. 2C). Eventually, in beta frequency band in the interictal SWD time window, ten modules were detected.

The list of regions of the detected modules from all time windows are presented in Supplementary Table 1.

3.2.2. Network communities before and during ictal discharges

In gamma and beta frequency bands, the same network modules as those detected before the interictal SWDs (i.e. during the pre-SWD-15, pre-SWD-10, and pre-SWD-5 time windows) were identified before the ictal SWDs. During the ictal SWD time window one additional module (to those seven modules in gamma band and eight in beta band from the preceding three time windows) was detected, the basal ganglia module, which comprised caudate, putamen, and pallidum (without thalamus) in both frequency bands (Fig. 2D). Eventually, in the ictal SWD time window, eight modules in gamma band and nine modules in beta band were identified.

3.3. Dynamic properties of network communities

3.3.1. Flexibility and controllability before and during interictal discharges

In gamma and beta frequency bands, no significant differences (all $p > 0.05$) were attested in flexibility and controllability (all $p > 0.05$) measures within the six modules detected in the pre-SWD-10 time window as compared to the pre-SWD-15 time window (Suppl. Figs. 1 and 2).

In gamma frequency band, within the fronto-parietal module identified in the pre-SWD-5 time window, opposite dynamics with significantly increasing flexibility ($F(1, 39) = 25.3$, $p < 0.001$) and decreasing controllability ($F(1, 39) = 55.3$, $p < 0.001$) were found when compared to the pre-SWD-15 and pre-SWD-10 time windows (Fig. 3A). Opposite dynamics of decreasing flexibility ($F(1, 39) = 11.9$, $p < 0.001$) and increasing controllability ($F(1, 39) = 10.1$, $p < 0.001$) were observed within the fronto-temporal module in the interictal SWD time window when compared to the preceding time windows (Fig. 3B).

In beta frequency band, during the pre-SWD-5 time window significantly decreasing flexibility ($F(1, 39) = 18.7$, $p < 0.001$; $F(1, 39) = 15.1$, $p < 0.001$) and increasing controllability ($F(1, 39) = 13.3$, $p < 0.001$; $F(1, 39) = 15.7$, $p < 0.001$) were found within the fronto-parietal and mesial fronto-parietal modules when compared to pre-SWD-15 and pre-SWD-10 time windows (Fig. 4A). Similarly, in the interictal SWD time window decreasing flexibility ($F(1, 39) = 9.2$, $p < 0.001$; $F(1, 39) =$

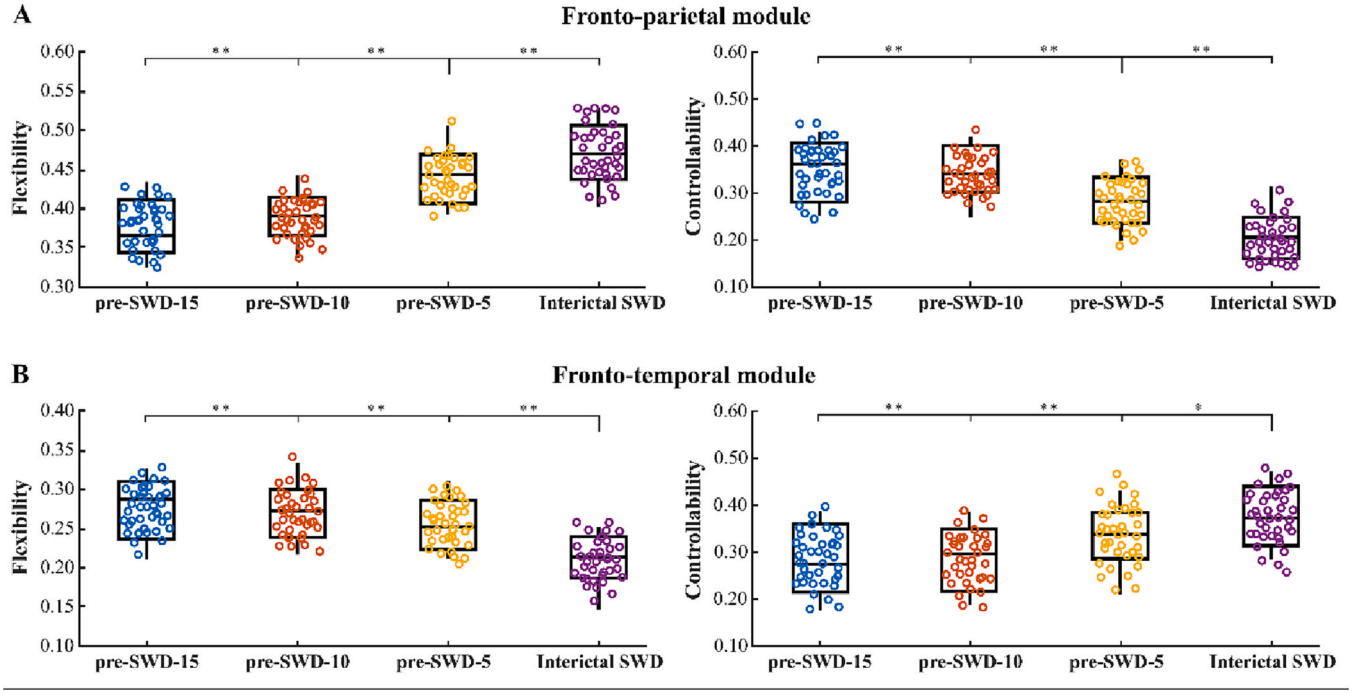

Fig. 3. Flexibility and controllability in the pre-SWD-5 and interictal SWD time windows (gamma band). Increasing flexibility and decreasing controllability within the fronto-parietal module from the pre-SWD-5 time window (A) and opposite dynamics within the fronto-temporal module from the interictal SWD time window (B); corrected for multiple comparisons $*p < 0.05$, $**p < 0.001$.

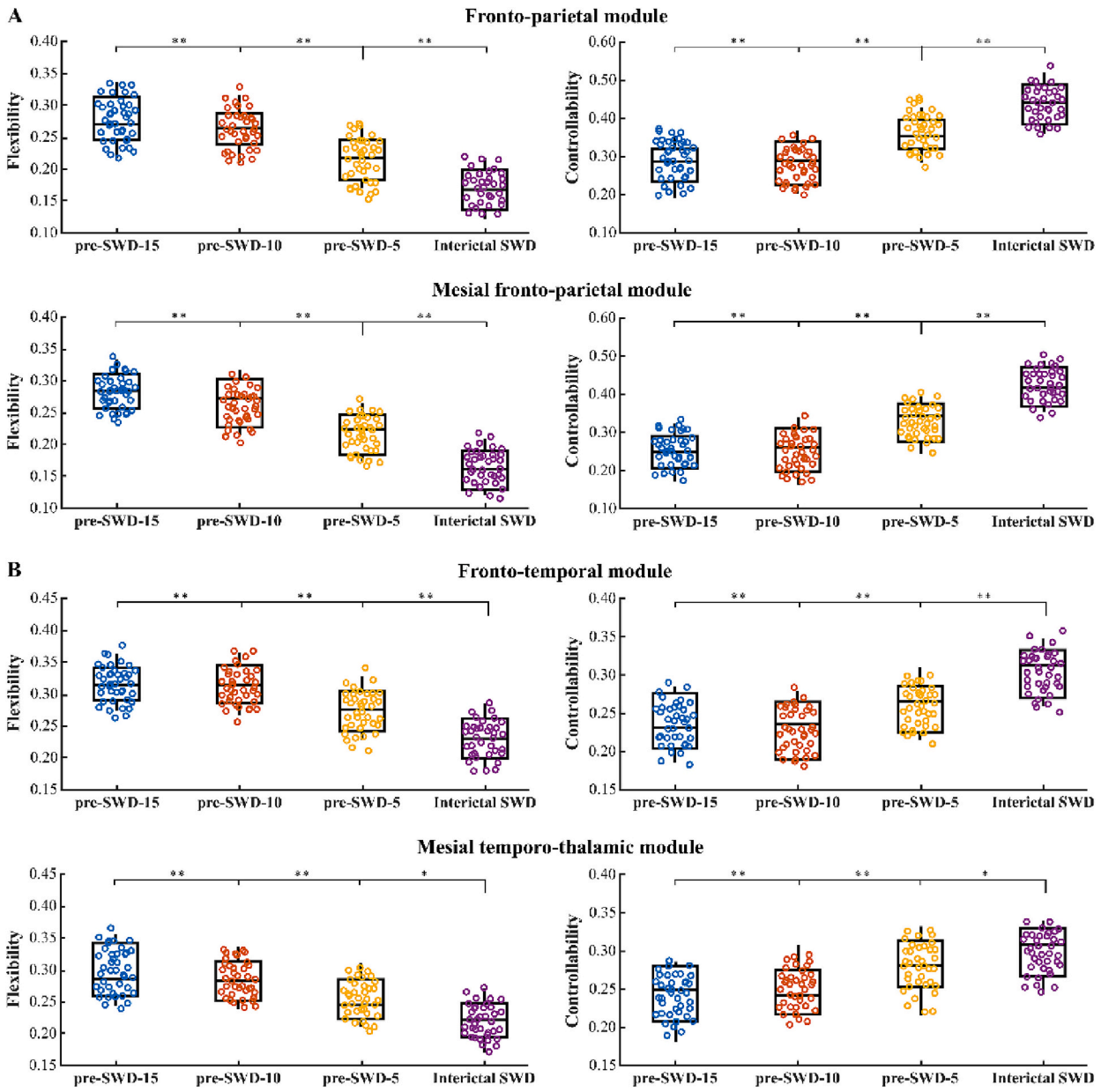

Fig. 4. Flexibility and controllability in the pre-SWD-5 and interictal SWD time windows (beta band). Decreasing flexibility and increasing controllability in fronto-parietal and mesial fronto-parietal modules in the pre-SWD-5 time window (A), and fronto-temporal and mesial temporo-thalamic modules in the interictal SWD time window (B); corrected for multiple comparisons *p < 0.05, **p < 0.001.

22.5, $p < 0.001$) and increasing controllability ($F(1, 39) = 14.7$, $p < 0.001$; $F(1, 39) = 8.8$, $p < 0.001$) were found within the fronto-temporal and mesial temporo-thalamic modules, when compared to the preceding three time windows (Fig. 4B).

3.3.2. *Flexibility and controllability before and during ictal discharges*

In gamma and beta frequency bands, no significant differences (all $p > 0.05$) were attested in flexibility and controllability (all $p > 0.05$) parameters within the six modules detected in the pre-SWD-10 time window as compared to the pre-SWD-15 time window (Suppl. Figs. 1 and 2).

In gamma frequency band, network alterations of the basal ganglia module in the ictal SWD time window were marked by decreasing flexibility ($F(1, 14) = 31.6$, $p < 0.001$) and increasing controllability ($F(1, 14) = 44.7$, $p < 0.001$) as compared to the prior time windows (Fig. 5A).

In beta frequency band, in the ictal SWD time window, again decreased flexibility ($F(1, 14) = 23.5$, $p < 0.001$) and increased controllability ($F(1, 14) = 31.1$, $p < 0.001$) were found within the basal ganglia module when compared to the prior time windows (Fig. 5B).

3.4. *Intermodular network topology*

3.4.1. *Network topology before and during interictal discharges*

No significant differences in clustering coefficient were attested between the modules in the pre-SWD-15 and pre-SWD-10 time windows in gamma and beta frequency bands (Suppl. Fig. 3).

A frequency-dependent opposite dynamics of clustering coefficient between the modules was observed across the four time windows. Thus, in gamma frequency band, a higher clustering coefficient between the modules identified in the pre-SWD-5 ($F(1, 39) = 4.6$, $p < 0.05$) and interictal SWD ($F(1, 39) = 9.2$, $p < 0.001$) time windows was observed when compared to the preceding time windows (Fig. 6A and B).

In beta frequency band, a lower clustering coefficient between the

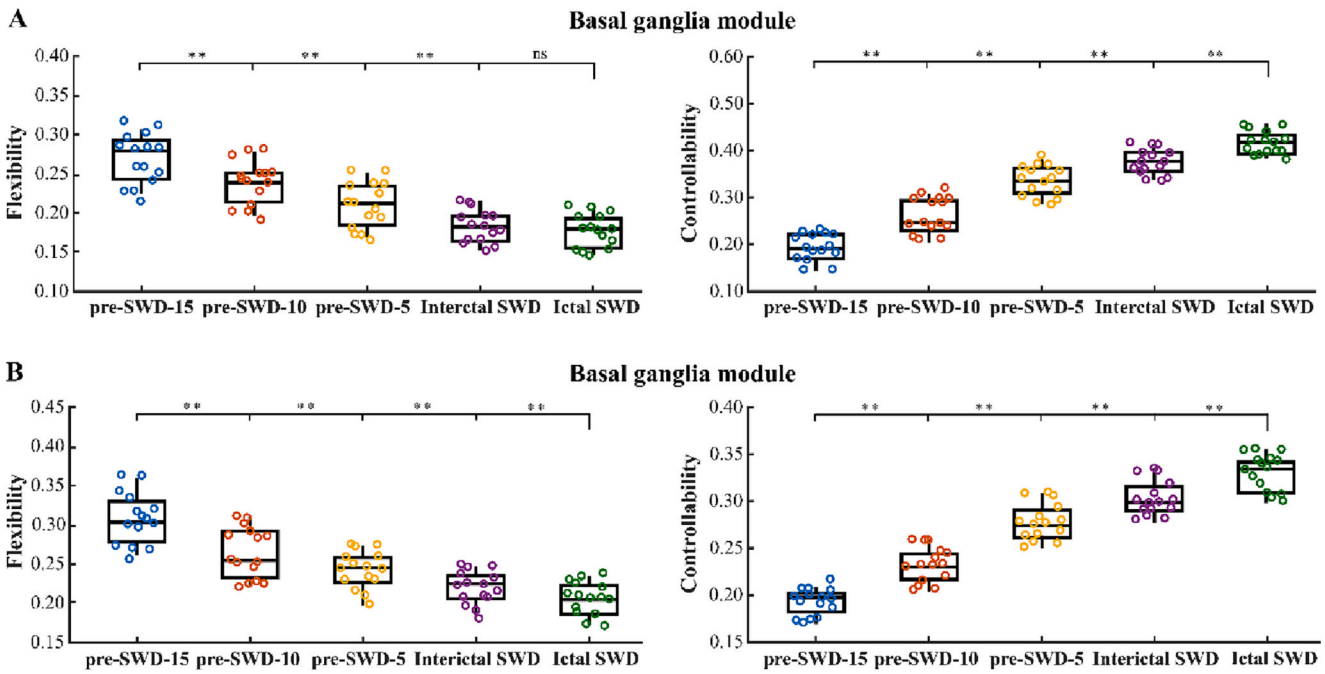

Fig. 5. Flexibility and controllability in the pre-SWD-5, interictal SWD, and ictal SWD time windows. Decreasing flexibility and increasing controllability within the basal ganglia module from the ictal SWD time window in gamma (A) and beta (B) frequency bands; corrected for multiple comparisons *p < 0.05, **p < 0.001.

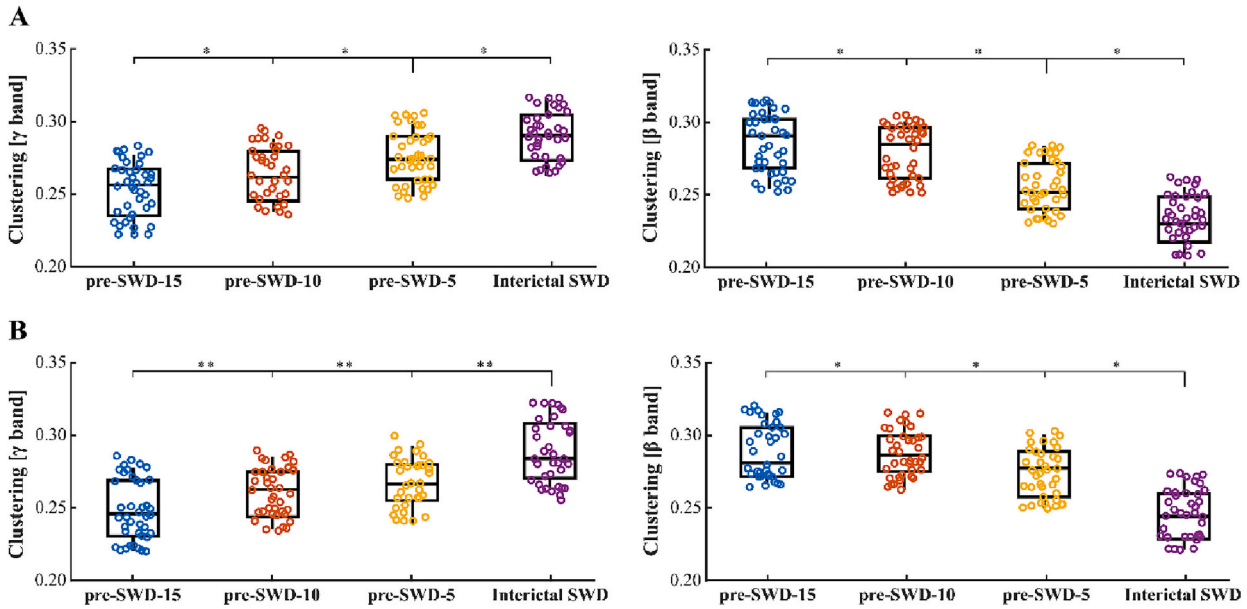

Fig. 6. Intermodular network topology in the pre-SWD-5 and interictal SWD time windows (gamma and beta bands). Clustering coefficient between the modules identified in the pre-SWD-5 (A) and interictal SWD (B) time windows as compared to the preceding time windows; corrected for multiple comparisons *p < 0.05, **p < 0.001.

modules identified in the pre-SWD-5 ($F(1, 39) = 2.5$, $p < 0.05$) and interictal SWD ($F(1, 39) = 6.9$, $p < 0.05$) time windows was found when compared to the preceding time windows (Fig. 6A and B).

3.4.2. *Network topology before and during ictal discharges*

In gamma frequency band, a higher clustering coefficient between the modules detected in the ictal SWD time window ($F(1, 14) = 58.8$, $p < 0.001$) was observed when compared to the prior time windows (Fig. 7).

In beta frequency band, a lower clustering coefficient between the modules detected in the ictal SWD time window ($F(1, 14) = 15.6$, $p < 0.001$) was found when compared to the preceding time windows, except for the interictal SWD time window (Fig. 7).

3.5. *Network dynamics relate to seizure frequency and cognitive status*

The frequency of myoclonic seizures was significantly associated with the flexibility ($r = 0.25$, $p = 0.03$; prediction accuracy 84%) and controllability ($r = -0.23$, $p = 0.03$; prediction accuracy 83%) within the interictal fronto-temporal module in beta band. The MoCA test was significantly associated with the flexibility ($r = -0.28$, $p = 0.04$; prediction accuracy 81%) and controllability ($r = 0.25$, $p = 0.03$; prediction

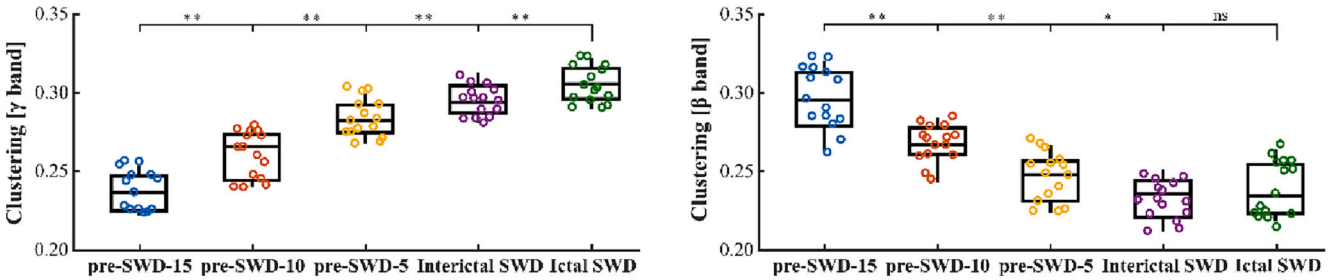

Fig. 7. Intermodular network topology in the ictal SWD time window (gamma and beta bands). Clustering coefficient between the modules identified in the ictal SWD time windows as compared to the preceding time windows; corrected for multiple comparisons **p < 0.001.

accuracy 77%) of the same interictal fronto-temporal module. A significant association between the HAM-A test and flexibility ($r = 0.23$, $p = 0.03$; prediction accuracy 84%) within the ictal basal ganglia module in gamma band was found. No statistically significant associations between other variables were attested.

4. Discussion

In this work, we investigated the organization and dynamic properties of network modules during the transition to interictal and ictal states in JME patients. We found several modules comprising specific cortical and subcortical regions depending on the analyzed time windows of the hdEEG recordings. Particularly, regions of the frontal and parietal lobes were more frequently involved in the time windows preceding the occurrence of interictal and ictal discharges (i.e. pre-SWD-15, pre-SWD-10, and pre-SWD-5 time windows) and basal ganglia (caudate, putamen, pallidum) during the ictal discharges (i.e. ictal SWD time window). Dynamic transformations within the identified modules were characterized by concomitantly decreasing flexibility and increasing controllability as brain activity evolved towards interictal and ictal SWDs.

One of the aims of the current study was to characterize the modular organization of brain networks, given its potential relevance for the generation and propagation of SWDs. Since physiological modular organization of brain networks contributes to an efficient integration of large-scale brain activities (Bertolero et al., 2018), it can been postulated that modular configuration of brain networks might also facilitate the emergence of SWDs in epileptic brains by enhancing the interregional synchronization. Indeed, according to the obtained results, patients with JME displayed clear modular structure of brain networks engaged in an aberrant oscillatory activity prior to and during SWD generation. In our JME population, cortical areas of the frontal (including mesial frontal), parietal (including precuneus), and temporal lobes along with the thalamus were the regions more commonly identified as parts of the network modules in the time windows preceding both interictal and ictal SWDs. The identified here brain network regions are concordant with the results of previous studies showing that sources of SWDs localize mainly to cortico(fronto)-thalamic network (Blumenfeld, 2005; Japaridze et al., 2016; En et al., 2002; Holmes et al., 2010). Also, multiple sources during the slow waves of the SWD complexes were localized to temporal, parietal, and occipital lobe regions (Moeller et al., 2008; En et al., 2002; Holmes et al., 2010). Mesial frontal and temporal lobe areas are considered as important drivers of SWDs (Holmes et al., 2010), while precuneal activation several seconds prior to SWDs may act as a gating mechanism for SWD generation (Vaudano et al., 2009; Lee et al., 2014). However, we found distinct modules during the occurrence of interictal and ictal SWDs – the fronto-temporal and mesial temporo-thalamic modules within the interictal SWD time window and basal ganglia module within the ictal SWD time window. Presence of the basal ganglia module within the ictal SWDs may suggest the propagation of epileptic activity towards the basal ganglia that translates into motor component of myoclonic seizures.

Brain networks undergo dynamic transformations as brain activity evolves to interictal or ictal discharges (Khambhati et al., 2015). We found higher flexibility estimates of network modules within the time windows preceding interictal and ictal SWDs as compared to flexibility estimates during the occurrence of interictal and ictal SWDs. These findings point to the possible reduction in the module communication frequency with other modules prior to the SWDs, thereby facilitating the occurrence of upcoming interictal or ictal discharges. Accordingly, higher network flexibility, reflecting desynchronized connectivity, prior to seizure occurrence has been suggested to drive the network to a more predictable series of increasingly synchronized states during the seizure (Khambhati et al., 2015). Patients with focal neocortical epilepsy display similar decrease in network flexibility as the networks evolve from the pre-seizure to seizure state (Khambhati et al., 2015). Increased network flexibility prior to ictal discharges may facilitate seizure generation through a rapid reorganization of weak (desynchronized) connections in the epileptic network. Thereby, during the ictal state, an even more decreased flexibility may reflect the redistribution of weak connectivity to a strong (synchronized) connectivity within the epileptic network. We found that the frequency of generalized myoclonic seizures was associated with flexibility within the fronto-temporal module of interictal SWDs but not within the basal ganglia module of ictal SWDs. The relation between the frequency of seizures (including myoclonic seizures) and interictal discharges (including generalized SWDs) was previously attested in generalized as well as in focal epilepsies (Ebus et al., 2012; Lv et al., 2013; Krendl et al., 2008; Janszky et al., 2005), suggesting that interictal events reflect a decreased seizure susceptibility and may lead to the occurrence of ictal activity and seizures (Janszky et al., 2005; Avoli, 2001). Possible explanations of this link might emerge from the evidence pointing that i) seizures increase the frequency of interictal discharges and ii) the network of the interictal activity is similar to the network of subsequent seizure activity (Janszky et al., 2005). As reported by recent studies, interictal discharges are bidirectional traveling waves echoing ictal discharges that traverse the same pathways as ictal discharges, suggesting a spatiotemporal similarity between interictal and ictal discharges (Smith et al., 2022). Thus, the identified here correlation between the flexibility within the interictal fronto-temporal module and seizure frequency may indicate that the dynamic reorganization of modules during interictal SWDs is relevant for upcoming precipitation of ictal SWDs and myoclonic seizures.

Network controllability may be a useful measure to assess the dynamics of abnormal brain activity during the transition to interictal or ictal discharges as it offers valuable insights into the spatio-temporal properties of evolving epileptic activity (Scheid et al., 2021). Opposite to the dynamics of flexibility, we found an increase in the network controllability as moving from the pre-SWD to interictal and ictal SWD time windows. Increasing controllability within the detected network communities preceding and during SWDs may indicate the increased propensity of these network communities to reach the hard-to-reach neurophysiological states such as seizure states. Strightforward, this propensity of directing the activity towards hard-to-reach brain states was greatest during the occurrence of both interictal and ictal

discharges. Similarly, patients with focal epilepsy display increase in network controllability beginning with preictal and throughout the ictal state (Scheid et al., 2021). Increasing controllability as reaching the ictal discharges, where synchrony also increases, suggests that it will become harder for controlling mechanisms to direct the brain activity into an energetically unfavorable state (Scheid et al., 2021). It is important to mention that the controlling mechanisms vary across the brain networks. We found that frontal and parietal regions were consistently detected as parts of network communities within the time windows preceding the SWDs. In line with existing data, regions with high controllability are usually enriched in fronto-parietal control networks (Gu et al., 2015). Thus, it is important not only to assess the dynamics of controllability during brain state transitions but also to map the regions responsible for executing the control mechanisms. Eventually, the presented findings indicate that strong dependency of network controllability during transitions to interictal and ictal discharges is a characteristic feature of evolving epileptic networks.

According to the obtained results, both flexibility and controllability showed similar dynamic alterations within the time windows prior to and during the occurrence of interictal and ictal SWDs. These findings point to common underlying pathophysiological network mechanisms involved in the generation of interictal and ictal SWDs, both originating within the cortico-thalamic circuits engaged in a bidirectional crosstalk, with the cortex and thalamus taking turns in driving each other (Lüttjohann and Pape, 2019). Interestingly, network alterations were attested only in gamma and beta frequency bands but not at lower (alpha, theta, delta) frequencies. The mechanistic underpinnings behind these observations are unclear, since existing evidence shows that coalescence of delta and theta frequencies in the cortex is favorable for the occurrence of SWDs (Sitnikova and van Luijtelaar, 2009). However, recent studies assign an important role to high frequency (13–60 Hz) oscillations in the synchronization of cortical and thalamic generators contributing to SWDs (Benedek et al., 2016). Increases in gamma and beta activity were accompanied by concomitant inhibition of alpha (4–8 Hz) activity, suggesting the predominance of inhibitory GABA-ergic mechanisms (Benedek et al., 2016). Hence, from our and other existing data, it might be assumed that gamma and beta oscillatory activity is relevant for the occurrence of interictal and ictal SWDs in IGE, including JME.

To characterize the dynamics of network connectivity between the modules we measured the clustering coefficient. A frequency-dependent opposite dynamics with decreasing clustering in beta band and increasing clustering in gamma band was observed across the analyzed time windows. Decreasing clustering in beta band may suggest reduced connectivity between the detected network modules, perhaps, reflecting network decoupling while approaching to interictal and ictal SWDs. The decreased connectivity between the modules was supported by the decrease of flexibility (indicating weak connections) within the modules. A study using lower EEG density (64-channels) and less JME patients ($n = 11$) reported similar reduction in clustering during SWD occurrence compared to the pre-SWD time window in beta and theta bands (Lee et al., 2017). Moreover, the described here dynamics of clustering are not characteristic only to JME patients, since comparable dynamics of clustering is observed during the transition to ictal state also in focal epilepsy patients –decreased clustering (network decoupling) during interictal and seizure state and increased clustering (network coupling) during seizure onset and offset (Kramer and Cash, 2012). Thus, observed findings on clustering indicate dynamic reorganization of inter-modular network connections during brain state transitions from the pre-SWD to interictal and ictal states that occur concomitantly along with intra-modular reorganization.

Some clinical implications emerge based on the obtained findings. Particularly, the observed network dynamics may potentially be useful to optimize the application of non-invasive neuromodulatory techniques and to advance the field of network-guided neuromodulation. Since the identified network modules comprise many cortical regions (mainly fronto-parietal and forno-temporal), a multifocal transcranial magnetic stimulation paradigm delivered over these areas (Leahu et al., 2021) may be more effective compared to previous unifocal paradigms focusing over the vertex region in IGE (Kimiskidis et al., 2014). This approach may be employed as an adjunctive seizure-preventive treatment in patients with drug-resistant JME. Similarly, the addressed network measures may improve the delivery of vagus nerve stimulation in refractory cases of IGE (Workewych et al., 2020), including JME. Despite the similar network dynamics prior to interictal and ictal SWDs, quantification of flexibility and/or of controllability measures may serve as prognostic markers of treatment response in JME patients. Thus, by assessing these network parameters, inferences on individual therapeutic response and clinical outcomes may be made. Given the evidence on the impact of abnormal network flexibility and interictal discharges on cognitive status (Tailby et al., 2018; Faught et al., 2018) in epilepsy patients, the identified here association between flexibility of the interictal fronto-temporal network module and cognitive performance, prompts a more close neuropsychological observation of JME patients with frequent occurrence of interictal SWDs.

This study does not go without limitations. First, in this study we did not estimate the specific localization of SWD sources, which is thoroughly reported in the literature (Moeller et al., 2008; En et al., 2002; Holmes et al., 2010) but rather employed a data-driven approach to extract the sources of whole-brain activity. Second, the obtained results describe the network communities and their properties evaluated at one time point and across all patients without providing characterization on intraindividual and interindividual variability of network alterations in JME patients. Given the stereotypical occurrence of SWDs in individual patients, a low intraindividual variablity across multiple SWDs can be assumed. Third, since in our study the community structure was extracted from EEG recordings, using data from other imaging, structural or functional, modalities may provide variations in the community structure. Future studies combining structural and functional data will offer complementary insights in characterizing the community structure and its dynamics in JME patients. Fourth, all patients were receiving antiseizure medications that might have potentially influenced the network measures. Therefore, variability of the received medication across patients was included as a confounding variable in the employed statistical models. Lastly, the utilized here approach assumes noise-free, linear network dynamics within each five seconds time window. Although the brain is not a linear system, linear approximations on a short timescale are able to capture broad dynamics in epilepsy while allowing for the application of controllability metrics.

5. Conclusions

By addressing the brain network abnormalities in patients with JME, we found a similar distribution pattern of network communities prior to the generation of both interictal and ictal SWDs as well as distinct pattern of communities during interictal and ictal SWDs. Dynamic alterations within the detected network communities were marked by decreased flexibility and increased controllability prior to and during both interictal SWDs and ictal SWDs in both gamma and beta frequency bands. These findings indicate that fluctuations in gamma and beta frequency could initiate a starting phenomenon in functional segregation which is further sustained by means of increased clustering. Timing and regional distribution of observed alterations in brain connectivity could support the elaboration of network-based biomarkers and more targeted neuromodulatory therapies in JME.

Funding

This study was supported by the German Research Foundation (DFG; CRC-TR-128) and by Nicolae Testemitanu State University of Medicine and Pharmacy (project codes 20.80009.8007.40 and 21.80013.8007.2B).

CRediT authorship contribution statement

Anatolie Vataman: Methodology, Investigation, Formal analysis, Writing – original draft, Writing – review & editing. **Dumitru Ciolac:** Formal analysis, Writing – original draft, Writing – review & editing, Visualization. **Vitalie Chiosa:** Writing – review & editing. **Daniela Aftene:** Writing – review & editing. **Pavel Leahu:** Writing – review & editing. **Yaroslav Winter:** Writing – review & editing. **Stanislav A. Groppa:** Supervision, Resources, Writing – review & editing, Project administration. **Gabriel Gonzalez-Escamilla:** Formal analysis, Writing – review & editing, Visualization. **Muthuraman Muthuraman:** Methodology, Software, Formal analysis, Visualization, Writing – review & editing. **Sergiu Groppa:** Conceptualization, Investigation, Supervision, Writing – review & editing, Project administration, Resources.

Declaration of Competing Interest

The authors report no competing interests.

Data availability

Data will be made available on request.

Acknowledgments

We thank Kathleen Claussen for proofreading the manuscript.

Appendix A. Supplementary data

Supplementary data to this article can be found online at https://doi.org/10.1016/j.nbd.2023.106055.

References

Assenza, G., Lanzone, J., Dubbioso, R., et al., 2020. Thalamic and cortical hyperexcitability in juvenile myoclonic epilepsy. Clin. Neurophysiol. 131 (8), 2041–2046.
Avoli, M., 2001. Do interictal discharges promote or control seizures? Experimental evidence from an in vitro model of epileptiform discharge. Epilepsia. 42, 2–4.
Bassett, D.S., Wymbs, N.F., Porter, M.A., Mucha, P.J., Carlson, J.M., Grafton, S.T., 2011. Dynamic reconfiguration of human brain networks during learning. Proc. Natl. Acad. Sci. 108 (18), 7641–7646.
Beck, A.T., Steer, R.A., Ball, R., Ranieri, W.F., 1996. Comparison of Beck depression inventories-IA and-II in psychiatric outpatients. J. Pers. Assess. 67 (3), 588–597.
Benedek, K., Berényi, A., Gombkötő, P., Piilgaard, H., Lauritzen, M., 2016. Neocortical gamma oscillations in idiopathic generalized epilepsy. Epilepsia. 57 (5), 796–804.
Beniczky, S., Guaranha, M.S.B., Conradsen, I., et al., 2012. Modulation of epileptiform EEG discharges in juvenile myoclonic epilepsy: an investigation of reflex epileptic traits. Epilepsia. 53 (5), 832–839.
Benuzzi, F., Mirandola, L., Pugnaghi, M., et al., 2012. Increased cortical BOLD signal anticipates generalized spike and wave discharges in adolescents and adults with idiopathic generalized epilepsies. Epilepsia. 53 (4), 622–630.
Bertolero, M.A., Yeo, B.T., Bassett, D.S., D'Esposito, M., 2018. A mechanistic model of connector hubs, modularity and cognition. Nat. Hum. Behav. 2 (10), 765–777.
Blondel, V.D., Guillaume, J.-L., Lambiotte, R., Lefebvre, E., 2008. Fast unfolding of communities in large networks. Journal of statistical mechanics: theory and experiment. 2008 (10), P10008.
Blumenfeld, H., 2005. Cellular and network mechanisms of spike-wave seizures. Epilepsia. 46, 21–33.
Caeyenberghs, K., Powell, H., Thomas, R.H., et al., 2015. Hyperconnectivity in juvenile myoclonic epilepsy: a network analysis. NeuroImage: Clinical. 7, 98–104.
Chiosa V, Groppa SA, Ciolac D, et al. Breakdown of Thalamo-cortical connectivity precedes spike generation in focal epilepsies. Brain connectivity. Jun 2017;7(5): 309–320. doi:https://doi.org/10.1089/brain.2017.0487.
Chiosa, V., Ciolac, D., Groppa, S., et al., 2019. Large-scale network architecture and associated structural cortico-subcortical abnormalities in patients with sleep/awake-related seizures. Sleep 42 (4), 1–9.
Clemens, B., Puskas, S., Besenyei, M., et al., 2013. Neurophysiology of juvenile myoclonic epilepsy: EEG-based network and graph analysis of the interictal and immediate preictal states. Epilepsy Res. 106 (3), 357–369.
Dähne, S., Meinecke, F.C., Haufe, S., et al., 2014. SPoC: a novel framework for relating the amplitude of neuronal oscillations to behaviorally relevant parameters. NeuroImage. 86, 111–122.
Ebus, S., Arends, J., Hendriksen, J., et al., 2012. Cognitive effects of interictal epileptiform discharges in children. Eur. J. Paediatr. Neurol. 16 (6), 697–706.
En, Santiago-Rodríguez, Ta, Harmony, Fernández-Bouzas, A., et al., 2002. Source analysis of polyspike and wave complexes in juvenile myoclonic epilepsy. Seizure. 11 (5), 320–324.
Faught, E., Karakis, I., Drane, D.L., 2018. The impact of interictal discharges on performance. Current Neurology and Neuroscience Reports. 18 (12), 1–9.
Gollo, L.L., Roberts, J.A., Cocchi, L., 2017. Mapping how local perturbations influence systems-level brain dynamics. Neuroimage. 160, 97–112.
Gonzalez-Escamilla, G., Chirumamilla Venkata, C., Koirala, N., et al., 2023. Modular segregation drives causality of the dynamic oscillatory network responses during threat processing. Brain Commun, fcad035. https://doi.org/10.1093/braincomms/fcad035 (in press).
Groppa, S., Siebner, H.R., Kurth, C., Stephani, U., Siniatchkin, M., Dec 2008. Abnormal response of motor cortex to photic stimulation in idiopathic generalized epilepsy. Epilepsia. 49 (12), 2022–2029. https://doi.org/10.1111/j.1528-1167.2008.01709.x.
Groppa, S., Moeller, F., Siebner, H., et al., Apr 2012. White matter microstructural changes of thalamocortical networks in photosensitivity and idiopathic generalized epilepsy. Epilepsia. 53 (4), 668–676. https://doi.org/10.1111/j.1528-1167.2012.03414.x.
Gu, S., Pasqualetti, F., Cieslak, M., et al., 2015. Controllability of structural brain networks. Nat. Commun. 6 (1), 1–10.
Gupta, D., Ossenblok, P., van Luijtelaar, G., 2011. Space–time network connectivity and cortical activations preceding spike wave discharges in human absence epilepsy: a MEG study. Medical & biological engineering & computing. 49 (5), 555–565.
Hamilton, M., 1959. The assessment of anxiety states by rating. Br. J. Med. Psychol. 32 (1), 50–55.
Holmes, M.D., Quiring, J., Tucker, D.M., 2010. Evidence that juvenile myoclonic epilepsy is a disorder of frontotemporal corticothalamic networks. Neuroimage. 49 (1), 80–93.
Janszky, J., Hoppe, M., Clemens, Z., et al., 2005. Spike frequency is dependent on epilepsy duration and seizure frequency in temporal lobe epilepsy. Epileptic disorders. 7 (4), 355–359.
Japaridze, G., Kasradze, S., Lomidze, G., et al., 2016. Focal EEG features and therapeutic response in patients with juvenile absence and myoclonic epilepsy. Clin. Neurophysiol. 127 (2), 1182–1187.
Jiang, S., Luo, C., Gong, J., et al., 2018. Aberrant thalamocortical connectivity in juvenile myoclonic epilepsy. Int. J. Neural Syst. 28 (01), 1750034.
Khambhati, A.N., Davis, K.A., Oommen, B.S., et al., 2015. Dynamic network drivers of seizure generation, propagation and termination in human neocortical epilepsy. PLoS Comput. Biol. 11 (12), e1004608.
Kimiskidis, V.K., Valentin, A., Kälviäinen, R., 2014. Transcranial magnetic stimulation for the diagnosis and treatment of epilepsy. Curr. Opin. Neurol. 27 (2), 236–241.
Kramer, M.A., Cash, S.S., 2012. Epilepsy as a disorder of cortical network organization. Neuroscientist 18 (4), 360–372.
Krendl, R., Lurger, S., Baumgartner, C., 2008. Absolute spike frequency predicts surgical outcome in TLE with unilateral hippocampal atrophy. Neurology. 71 (6), 413–418.
Leahu, P., Bange, M., Ciolac, D., et al., 2021. Increased migraine-free intervals with multifocal repetitive transcranial magnetic stimulation. Brain stimulation. 14 (6), 1544–1552.
Lee, C., Kim, S.-M., Jung, Y.-J., Im, C.-H., Kim, D.W., Jung, K.-Y., 2014. Causal influence of epileptic network during spike-and-wave discharge in juvenile myoclonic epilepsy. Epilepsy Res. 108 (2), 257–266.
Lee, C., Im, C.-H., Koo, Y.S., et al., 2017. Altered network characteristics of spike-wave discharges in juvenile myoclonic epilepsy. Clinical EEG and neuroscience. 48 (2), 111–117.
Liu, C., Crone, N., Franaszczuk, P., Cheng, D., Schretlen, D., Lenz, F., 2011. Fear conditioning is associated with dynamic directed functional interactions between and within the human amygdala, hippocampus, and frontal lobe. Neuroscience. 189, 359–369.
Lüttjohann, A., Pape, H.-C., 2019. Regional specificity of cortico-thalamic coupling strength and directionality during waxing and waning of spike and wave discharges. Sci. Rep. 9 (1), 1–11.
Lv, Y., Wang, Z., Cui, L., Ma, D., Meng, H., 2013. Cognitive correlates of interictal epileptiform discharges in adult patients with epilepsy in China. Epilepsy Behav. 29 (1), 205–210.
Mader, M., Mader, W., Sommerlade, L., Timmer, J., Schelter, B., 2013. Block-bootstrapping for noisy data. J. Neurosci. Methods 219 (2), 285–291.
Moeller, F., Siebner, H.R., Wolff, S., et al., 2008. Changes in activity of striato–thalamo–cortical network precede generalized spike wave discharges. Neuroimage. 39 (4), 1839–1849.
Moeller, F., Muthuraman, M., Stephani, U., Deuschl, G., Raethjen, J., Siniatchkin, M., 2013. Representation and propagation of epileptic activity in absences and generalized photoparoxysmal responses. Hum. Brain Mapp. 34 (8), 1896–1909.
Nasreddine, Z.S., Phillips, N.A., Bédirian, V., et al., 2005. The Montreal cognitive assessment, MoCA: a brief screening tool for mild cognitive impairment. J. Am. Geriatr. Soc. 53 (4), 695–699.
O'Muircheartaigh, J., Vollmar, C., Barker, G.J., et al., 2012. Abnormal thalamocortical structural and functional connectivity in juvenile myoclonic epilepsy. Brain. 135 (12), 3635–3644.
Onnela, J.-P., Saramäki, J., Kertész, J., Kaski, K., 2005. Intensity and coherence of motifs in weighted complex networks. Phys. Rev. E 71 (6), 065103.
Oostenveld, R., Fries, P., Maris, E., Schoffelen, J.-M., 2011. FieldTrip: open source software for advanced analysis of MEG, EEG, and invasive electrophysiological data. Computational intelligence and neuroscience. 2011.
Ritchey, M., Yonelinas, A.P., Ranganath, C., 2014. Functional connectivity relationships predict similarities in task activation and pattern information during associative memory encoding. J. Cogn. Neurosci. 26 (5), 1085–1099.

Rubinov, M., Sporns, O., 2010. Complex network measures of brain connectivity: uses and interpretations. Neuroimage. 52 (3), 1059–1069.
Sabbagh, D., Ablin, P., Varoquaux, G., Gramfort, A., Engemann, D.A., 2020. Predictive regression modeling with MEG/EEG: from source power to signals and cognitive states. NeuroImage. 222, 116893.
Scheffer, I.E., Berkovic, S., Capovilla, G., et al., Apr 2017. ILAE classification of the epilepsies: position paper of the ILAE Commission for Classification and Terminology. Epilepsia. 58 (4), 512–521. https://doi.org/10.1111/epi.13709.
Scheid, B.H., Ashourvan, A., Stiso, J., et al., 2021. Time-evolving controllability of effective connectivity networks during seizure progression. Proc. Natl. Acad. Sci. 118 (5), e2006436118 https://doi.org/10.1073/pnas.2006436118.
Sitnikova, E., van Luijtelaar, G., 2009. Electroencephalographic precursors of spike-wave discharges in a genetic rat model of absence epilepsy: power spectrum and coherence EEG analyses. Epilepsy Res. 84 (2–3), 159–171.
Sizemore, A.E., Bassett, D.S., 2018. Dynamic graph metrics: tutorial, toolbox, and tale. NeuroImage. 180, 417–427.
Smith, E.H., Liou, J.-y., Merricks, E.M., et al., 2022. Human interictal epileptiform discharges are bidirectional traveling waves echoing ictal discharges. Elife. 11, e73541.
Swami, P., Bhatia, M., Tripathi, M., Chandra, P.S., Panigrahi, B.K., Gandhi, T.K., Oct 2019. Selection of optimum frequency bands for detection of epileptiform patterns. Healthc Technol Lett. 6 (5), 126–131. https://doi.org/10.1049/htl.2018.5051.
Tailby, C., Kowalczyk, M.A., Jackson, G.D., 2018. Cognitive impairment in epilepsy: the role of reduced network flexibility. Annals of clinical and translational neurology. 5 (1), 29–40.
Tangwiriyasakul, C., Perani, S., Centeno, M., et al., 2018. Dynamic brain network states in human generalized spike-wave discharges. Brain. 141 (10), 2981–2994.
Trenité, D.G.K.-N., Schmitz, B., Janz, D., et al., 2013. Consensus on diagnosis and management of JME: from founder's observations to current trends. Epilepsy Behav. 28, S87–S90.
Van Veen, B.D., van Drongelen, W., Yuchtman, M., Suzuki, A., 1997. Localization of brain electrical activity via linearly constrained minimum variance spatial filtering. IEEE Trans. Biomed. Eng. 44 (9), 867–880. https://doi.org/10.1109/10.623056.
Vaudano, A.E., Laufs, H., Kiebel, S.J., et al., 2009. Causal hierarchy within the thalamo-cortical network in spike and wave discharges. PLoS One 4 (8), e6475.
Wolters, C.H., Anwander, A., Berti, G., Hartmann, U., 2007. Geometry-adapted hexahedral meshes improve accuracy of finite-element-method-based EEG source analysis. IEEE Trans. Biomed. Eng. 54 (8), 1446–1453.
Workewych, A.M., Arski, O.N., Mithani, K., Ibrahim, G.M., 2020. Biomarkers of seizure response to vagus nerve stimulation: a scoping review. Epilepsia. 61 (10), 2069–2085.
Zhang, Y., Guo, Y., Yang, P., Chen, W., Lo, B., 2019. Epilepsy seizure prediction on EEG using common spatial pattern and convolutional neural network. IEEE Journal of Biomedical and Health Informatics. 24 (2), 465–474.